

# Temporal evolution and source apportionment of BC aerosols during autumn in the grassland of Ordos, China

Yanhong Li<sup>1</sup> | Jinwen Zhang<sup>1</sup> | Qiyong Duan<sup>1</sup> | Xiangchen Kong<sup>1,2</sup> |  
 Honglei Wang<sup>3</sup> 

<sup>1</sup>Etuoke Banner Meteorological Bureau of Inner Mongolia, Ordos, China

<sup>2</sup>Collaborative Innovation Center of Atmospheric Environment and Equipment Technology, Jiangsu Key Laboratory of Atmospheric Environment Monitoring and Pollution Control (AEMPC), Nanjing University of Information Science & Technology, Nanjing, China

<sup>3</sup>China Meteorological Administration Aerosol-Cloud and Precipitation Key Laboratory, Nanjing University of Information Science and Technology, Nanjing, China

## Correspondence

Xiangchen Kong, Etuoke Banner Meteorological Bureau of Inner Mongolia, Ordos 017000, China.

Email: [15147736650@sina.cn](mailto:15147736650@sina.cn)

Honglei Wang, China Meteorological Administration Aerosol-Cloud and Precipitation Key Laboratory, Nanjing University of Information Science and Technology, Nanjing 210044, China.

Email: [hongleiwang@nuiist.edu.cn](mailto:hongleiwang@nuiist.edu.cn)

## Funding information

National Natural Science Foundation of China, Grant/Award Numbers: 42275196, 41830965; Natural Science Foundation of Jiangsu Province, Grant/Award Number: BK20231300; Wuxi University Research Start-up Fund for Introduced Talents, Grant/Award Number: 2023r035; Open fund by Jiangsu Key Laboratory of Atmospheric Environment Monitoring and Pollution Control, Grant/Award Number: KHK2207

## Abstract

Meteorological conditions and source emissions in grassland areas are quite different from those in urban areas, which significantly impacts the spatiotemporal characteristics of black carbon (BC). To obtain the characteristics of BC in the typical grassland environment in China, continuous observations of BC were carried out in Etuoke Banner, a typical grassland environment in Ordos, from September 8 to December 1, 2022. BC in Etuoke Banner in autumn is  $22.4\text{--}4667.5 \text{ ng m}^{-3}$ , and the average concentration is  $456.6 \text{ ng m}^{-3}$ , accounting for 2.20% of the mass fraction of  $\text{PM}_{2.5}$ .  $\text{BC}_{\text{liquid}}$  (BC generated from the combustion of liquid fuels) is the main component of BC (accounting for 79.2%); the average concentration is  $361.7 \text{ ng m}^{-3}$ . The diurnal variations of BC,  $\text{BC}_{\text{liquid}}$ , and  $\text{BC}_{\text{solid}}$  (BC generated from the combustion of solid fuels) are bimodal, with peaks at 08:00 and 18:00. The first peak is mainly related to traffic sources, cooking sources, and incomplete combustion of carbon-containing substances; the second peak may be caused by emissions from residential cooking sources under the influence of meteorological conditions unfavorable to diffusion. The diurnal variation of absorption Ångström exponent (AAE) is unimodal, with the peak at 14:00. With the increase in BC mass concentration, AAE and visibility gradually decreased, wind speed first decreased and then increased, P and RH gradually increased, and the contribution of biomass combustion sources to BC decreased. In contrast, the contribution of traffic sources to BC increased. The evolution characteristics of atmospheric pollutants differed with the increase in BC concentration. The potential sources and affecting areas of BC and  $\text{PM}_{2.5}$  are mainly concentrated around Etuoke Banner and can affect the North China Plain after 48 h of transmission.

## KEY WORDS

BC, diurnal variation, Etuoke Banner, grassland environment, source appointment

## 1 | INTRODUCTION

Black carbon (BC) is the most important absorbing aerosol, mainly derived from the incomplete combustion process of carbonaceous substances such as fossil fuels (petroleum and coal, etc.) and biomass (Ni et al., 2014; Shrestha et al., 2010; Zhang et al., 2015). BC accounts for a small proportion of the mass concentration of PM<sub>2.5</sub>, generally a few percent to more than 10%, but its strong absorption of solar radiation makes its ability to heat the atmosphere second only to greenhouse gases such as CO<sub>2</sub> (Chung & Seinfeld, 2005; Tan et al., 2022). BC's physical and chemical properties are relatively stable, and it is difficult to undergo chemical processes with other substances in the atmosphere. Still, its loose and porous structure is very conducive to adsorbing other pollutants and providing them with places and catalytic conditions for atmospheric chemical reactions (Atamny et al., 1992; Wang, Ke, et al., 2023; Zhu et al., 2023). BC can alter the boundary layer structure in urban areas, affecting the atmospheric pollution process (Li et al., 2017; Slater et al., 2022; Tan et al., 2020). BC can also adsorb toxic and harmful substances, affecting human health (Chen, Cheng, et al., 2023; Li et al., 2016).

The BC source emission characteristics have apparent temporal and spatial differences (Kant et al., 2023; Lim et al., 2023; Shen, Wang, Kong, Yin, et al., 2021; Shen, Wang, Kong, Zhang, et al., 2021). In the urban agglomeration area, the anthropogenic emissions are dense, and the BC mass concentration is high, which is also the area that the current global BC research focuses on (Roostaei et al., 2023; Rosa et al., 2014; Safai et al., 2007; Talukdar & Ratnam, 2023; Venkatachari et al., 2006). In the past few decades, numerous studies have focused on the temporal and spatial distribution characteristics, transmission mechanism, source–sink relationship, and health risk effects of BC in urban areas (Friedman et al., 2023; Gu et al., 2020; Lei et al., 2023; Liu et al., 2018; Shen, Wang, Kong, Yin, et al., 2021; Shen, Wang, Kong, Zhang, et al., 2021; Tripathi et al., 2005). Ozdemir et al. (2014) found that diurnal variations of BC concentrations and traffic density significantly correlate in Istanbul. Schleicher et al. (2013) indicated that BC was highest in winter due to Beijing's meteorological conditions and heating activities. Pani et al. (2020) found that biomass burning contributes as high as 92% to daily BC concentration. Liakakou et al. (2020) studied the remarkable effects of low wind speed and mixing-layer height in BC levels in Athens, Greece.

In China, numerous in-depth studies on the characteristics of BC pollution have been carried out in dense urban agglomeration areas such as the North China Plain (NCP) region, the Yangtze River Delta (YRD) region, the Pearl River Delta (PRD) region,

the Twain-Hu Basin, and the Sichuan Basin (Chen, Zhao, et al., 2023; Lin et al., 2019; Pei et al., 2022; Wan et al., 2023; Wei et al., 2023; Yang et al., 2022; Yuan et al., 2022; Zhang et al., 2023; Zheng et al., 2022). Yang et al. (2022) found that the refractory BC (rBC) core mass size distribution was bimodal, with a small secondary mode at ~687 nm in NCP. Zhang et al. (2021) investigated the light absorption of BC and rBC in six Chinese megacities in winter and found that rBC dominated the total  $b_{abs}$  in the northern cities. In contrast, BC was highly attributed to total  $b_{abs}$  in southern cities. Wang, Ke, et al. (2023) found that the heating effect of BC increases  $T$ , and the bottom height of the inversion layer (BHIL) elevates in Nanjing.

BC is chemically stable and can only be removed from the atmosphere through atmospheric dry and wet deposition. The lifetime of BC in the atmosphere lasts from days to weeks and then be transported over long distances (Liu et al., 2023; Lu et al., 2023; Ni et al., 2014; Shrestha et al., 2010; Zhang et al., 2015). BC will increase rapidly in haze, and the visibility will decrease sharply. BC can heat the upper atmosphere of the atmospheric boundary layer (ABL), making the ABL structure more stable, thereby exacerbating haze pollution (Ding et al., 2016; Xin et al., 2023). Zhao et al. (2020) found that the coatings of BC particles in the haze boundary layer can increase the atmospheric heating rate by 0.1 K h<sup>-1</sup> through aircraft observations since BC cannot react with other pollutants and is used as an excellent atmospheric tracer to explore the regional transport mechanism of pollutants (Aruna et al., 2013; Forbes et al., 2006; Gramsch et al., 2020; Hirdman et al., 2010; Shores et al., 2013; Wang, Liu, et al., 2023).

In grassland areas, where there are fewer anthropogenic emissions of air pollution, the pollution characteristics of BC are significantly different from urban areas. The source emissions of BC in grassland areas are also significantly different from those in urban areas, and animal grazing and wildfire burning are the primary sources in grassland areas (Emerson et al., 2018; Hao et al., 2016; Rodionov et al., 2010; Ulevicius et al., 2016). The Inner Mongolia Autonomous Region is the most essential grassland area in China. Much in-depth research has been conducted on the spatiotemporal distribution, transport mechanism, and source–sink relationship of aerosols in this area (Gao et al., 2023; Park & Park, 2014; Tan et al., 2012; Xie et al., 2023; Xu et al., 2015). However, there are relatively few studies on BC in this area. Ordos City is also located in the west of the NCP region. Under atmospheric circulation, the aerosols in this area can be transported to the NCP region. Therefore, the study of BC in Ordos City is also conducive to deepening our understanding of the characteristics of atmospheric

aerosol in the NCP region. To obtain the characteristics of BC in the typical grassland environment in China, we used a seven-channel aethalometer (AE-33) to continuously observe BC in Etuoke Banner, a specific grassland environment in Ordos, from September 8 to December 1, 2022. Combined with air pollution ( $\text{PM}_{10}$ ,  $\text{PM}_{2.5}$ ,  $\text{O}_3$ ,  $\text{SO}_2$ ,  $\text{NO}_2$ , and CO) data and meteorological data, the temporal characteristics of BC and its influencing factors were analyzed.

## 2 | MATERIALS AND METHODS

### 2.1 | Observation site

The observation site is in the Meteorological Bureau of Etuoke Banner ( $39.05^\circ \text{N}$ ,  $107.57^\circ \text{E}$ , altitude 1381.4 m) west of Ordos, Inner Mongolia Autonomous Region. Etuoke Banner has a total area of  $21,000 \text{ km}^2$ . The terrain is dominated by undulating plateaus, with high northwest and low southeast, an average altitude of 1800 m, and the typically temperate continental monsoon climate. Grasslands dominate the underlying surface. The total area of grassland resources is  $19,710 \text{ km}^2$ , accounting for 94% of the total land area in Etuoke Banner. Meteorological data include temperature, visibility, wind speed/direction, RH, and atmospheric pressure and precipitation; time resolution is 1 h. Six environmental factors ( $\text{PM}_{10}$ ,  $\text{PM}_{2.5}$ ,  $\text{NO}_2$ ,  $\text{SO}_2$ ,  $\text{O}_3$ , and CO) were provided by the China Environmental Observation Network (<http://106.37.208.233:20035/>), and the time resolution is 1 h. BC was observed using AE-33 with a time resolution of 5 min. The observation time is from September 8 to December 1, 2022.

The quality assurance and controls of six environmental factors data were implemented based on HJ 630-2011 specifications before releasing data; a detailed introduction can be found in (Zhao et al., 2016). Quality control for the meteorological dataset was implemented based on the surface observation criteria of the China Meteorological Administration. The BC data were inspected using the 3 $\delta$  method for quality control.

### 2.2 | Instruments and methods

BC mass concentrations were observed by an aethalometer with Model AE-33 (Magee Scientific, USA). Please refer to the literature for the instrument's principle detailed introduction (Chen et al., 2022). The BC's optical absorption at 880 nm can be attributed to the contribution of liquid fuel (vehicle exhausts) and solid fuel (coal and biomass combustion) (Zhang et al., 2009).  $\text{BC}_{\text{liquid}}$

and  $\text{BC}_{\text{solid}}$  can be calculated using the aethalometer model. The aerosol optical depth (AOD) data were obtained from NASA's Moderate Resolution Imaging Spectroradiometer (MODIS) instrument: BC surface mass concentrations, BC anthropogenic emissions, and biomass-burning emissions data provided by MERRA-2. The potential sources and areas affecting BC and  $\text{PM}_{2.5}$  can be calculated through potential source contribution function (PSCF) and concentration-weighted trajectory (CWT) models. Detailed introduction of instruments and methods is provided in the [Supporting information](#).

## 3 | RESULTS AND DISCUSSION

### 3.1 | Observation overview

Table 1 indicates that the BC mass concentration was  $22.4\text{--}4667.5 \text{ ng m}^{-3}$  in Etuoke Banner, with an average value of  $456.6 \text{ ng m}^{-3}$ , accounting for 2.20% of the mass fraction of  $\text{PM}_{2.5}$ . The BC mass concentration in Etuoke Banner is much lower than that in Beijing (Liu et al., 2018), Nanjing (Shen, Wang, Kong, Zhang, et al., 2021), Guangzhou (Lin et al., 2019), Wuhan (Zheng et al., 2022), and Chengdu (Yuan et al., 2022), and even lower than that in Litang on the eastern Qinghai-Tibet Plateau (Wang, Liu, et al., 2023).  $\text{BC}_{\text{liquid}}$ , as the main component of BC, has an average value of  $361.7 \text{ ng m}^{-3}$  in Etuoke Banner, approximately 79.2% of BC. Both AOD and BC surface mass concentration over Etuoke Banner have a low-value center (Figure 1), which is mainly because grasslands dominate the underlying surface of Etuoke Banner, and there are few anthropogenic emission sources around the sampling site, so the mass concentration of air pollutants is relatively low. Figure 1 indicates a few anthropogenic and biomass-burning emissions of BC around Etuoke Banner. Although Etuoke Banner is the underlying surface of the grassland, the grassland is mainly used as pasture, and there are almost no grassland wildfires so it can represent clean inland areas.

The  $\text{PM}_{2.5}$  and  $\text{PM}_{10}$  have relatively low mass concentrations in Etuoke Banner, with average values of 20.8 and  $58.4 \mu\text{g m}^{-3}$ , respectively (Table 1), and a  $\text{PM}_{2.5}/\text{PM}_{10}$  ratio of 35.6%. Affected by sandstorms, the maximum concentrations of  $\text{PM}_{2.5}$  and  $\text{PM}_{10}$  were 166 and  $1248 \mu\text{g m}^{-3}$  during the observation period, respectively. The lower PM indicates weaker aerosol extinction, which led to higher visibility (average value is 26.6 km) in the region.

The average value of temperature was  $7.3^\circ\text{C}$  in the observation period, the highest temperature was  $26.4^\circ\text{C}$ , and the  $\text{O}_3$  was low (average value was  $59.8 \mu\text{g m}^{-3}$ ). CO,

Factors	Maximum	Minimum	Average	Standard deviation
BC ( $\text{ng m}^{-3}$ )	4667.5	22.4	456.6	376.3
BC <sub>liquid</sub> ( $\text{ng m}^{-3}$ )	4064.4	12.9	361.7	329.7
BC <sub>solid</sub> ( $\text{ng m}^{-3}$ )	677.1	0.2	94.9	84.3
AAE	3.5	1.1	1.5	0.3
P	0.95	0.08	0.79	0.20
PM <sub>2.5</sub> ( $\mu\text{g m}^{-3}$ )	166	3	20.8	13.9
PM <sub>10</sub> ( $\mu\text{g m}^{-3}$ )	1248	3	58.4	52.2
O <sub>3</sub> ( $\mu\text{g m}^{-3}$ )	184	6	59.8	33.7
NO <sub>2</sub> ( $\mu\text{g m}^{-3}$ )	81	4	27.9	15.2
SO <sub>2</sub> ( $\mu\text{g m}^{-3}$ )	115	4	11.6	9.7
CO ( $\text{mg m}^{-3}$ )	1.34	0.32	0.64	0.18
T (°C)	26.4	-24.0	7.3	9.0
RH (%)	100.0	9.0	54.2	23.3
Visibility (km)	30.0	0.3	26.6	7.0
Wind speed ( $\text{m s}^{-1}$ )	9.5	0.2	2.4	1.7

Abbreviations: AAE, absorption Ångström exponent; BC, black carbon.

**TABLE 1** Summary of the atmospheric pollutants and meteorological elements during the observation period.

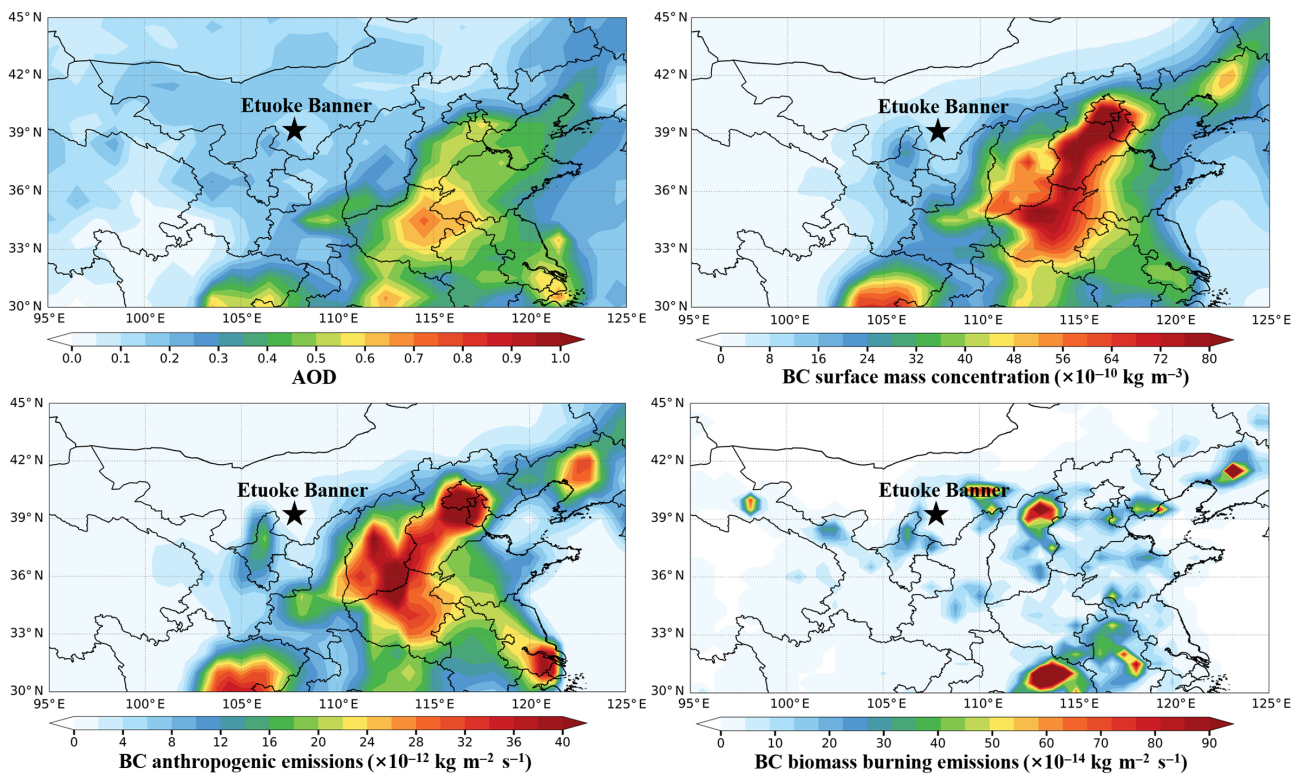


**FIGURE 1** Spatial distribution of aerosol optical depth, surface black carbon (BC) mass concentration, and primary emission sources of BC during the observation period.

SO<sub>2</sub>, and NO<sub>2</sub> were low, with average values of 0.64  $\text{mg m}^{-3}$ , 11.6, and 27.9  $\mu\text{g m}^{-3}$ , respectively. This is mainly due to the small population of Etuoke Banner, only 164,000, and less anthropogenic emissions; plains dominate the terrain, and the significant wind speed

(0.2–9.5  $\text{m s}^{-1}$ ) is beneficial to the diffusion of atmospheric pollutants, so the mass concentration of anthropogenic pollutants is lower.

Although BC and PM<sub>2.5</sub> had low mass concentrations in Etuoke Banner during the observation period, they

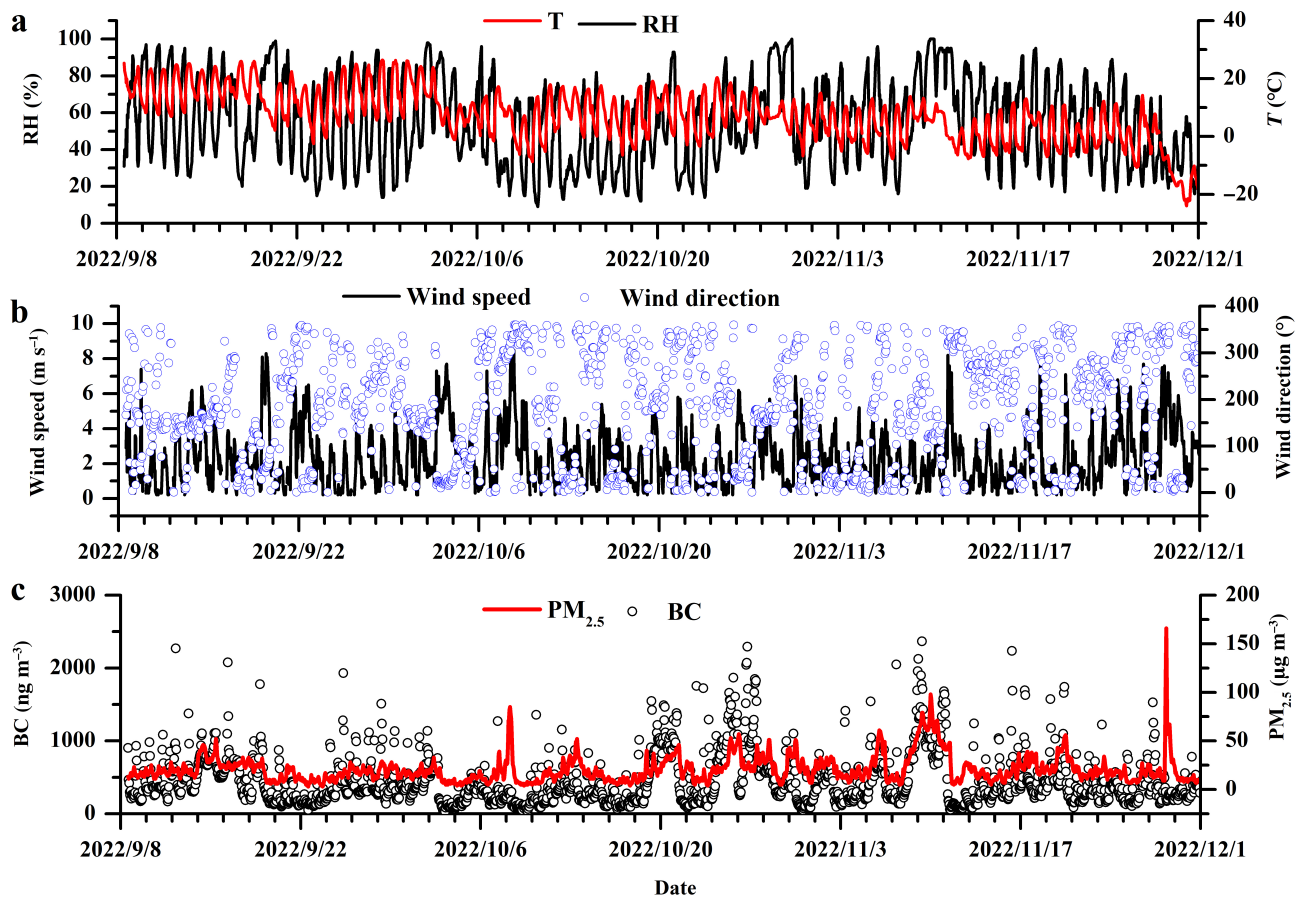


FIGURE 2 Time series of PM<sub>2.5</sub>, black carbon, and meteorological elements during the observation period.

fluctuated wildly over time (Figure 2). Figure 2 indicates that the BC mass concentration was relatively high during October 19–30 and November 5–7. The mass concentration is more than 800 ng m<sup>-3</sup>. During this period, the lower wind speed is conducive to accumulating atmospheric pollutants. The fluctuation of PM<sub>2.5</sub> mass concentration is relatively small, except for the high mass concentration in the sandstorm event on November 28; the mass concentration is low for the rest of the time. During the observation period, the wind direction of Etuoke Banner changed significantly; there was no apparent dominant wind direction, and the temperature difference between day and night was significant (Figure 2). The diurnal variation of RH is relatively large; it is lower at noon and less than 40%. Still, it is higher in the early morning, more than 80%, mainly caused by the underlying surface of the grassland.

The source of BC can be easily judged by correlation analysis with other pollutants. Figure 3 shows that BC has the best correlation with PM<sub>2.5</sub> and CO, and the coefficients of correlation (*R*) are 0.46 and 0.51, respectively, indicating that BC has similar sources with PM<sub>2.5</sub> and CO. BC correlates best with CO, originating primarily from combustion processes. The correlation between BC

and SO<sub>2</sub> is the worst; the correlation coefficient is only 0.12, and most of SO<sub>2</sub> comes from industrial emissions, which indicates that BC in Etuoke Banner does not come from industrial emissions. The *R* between BC and NO<sub>2</sub> is 0.30, which is weaker than that with PM<sub>2.5</sub> and CO, which indicates that the traffic source emission is not the principal source of BC in Etuoke Banner.

### 3.2 | Diurnal variations of BC and major atmospheric pollutants

Figure 4 indicates that the diurnal changes in BC are a typical bimodal distribution, with the peaks at 08:00 (China Standard Time, CST) and 18:00, respectively. There is an evident bimodal diurnal variation in SO<sub>2</sub> (Figure 5), with the peaks located at 09:00 and 21:00, respectively, which is not consistent with the morning peak time of BC, which also indicates that industrial source emissions are not the primary sources of BC in Etuoke Banner. NO<sub>2</sub> also showed an apparent bimodal distribution (Figure 5). The morning peak was located at 08:00, which was consistent with the variation of the morning peak in BC (Figure 4). The mass concentration

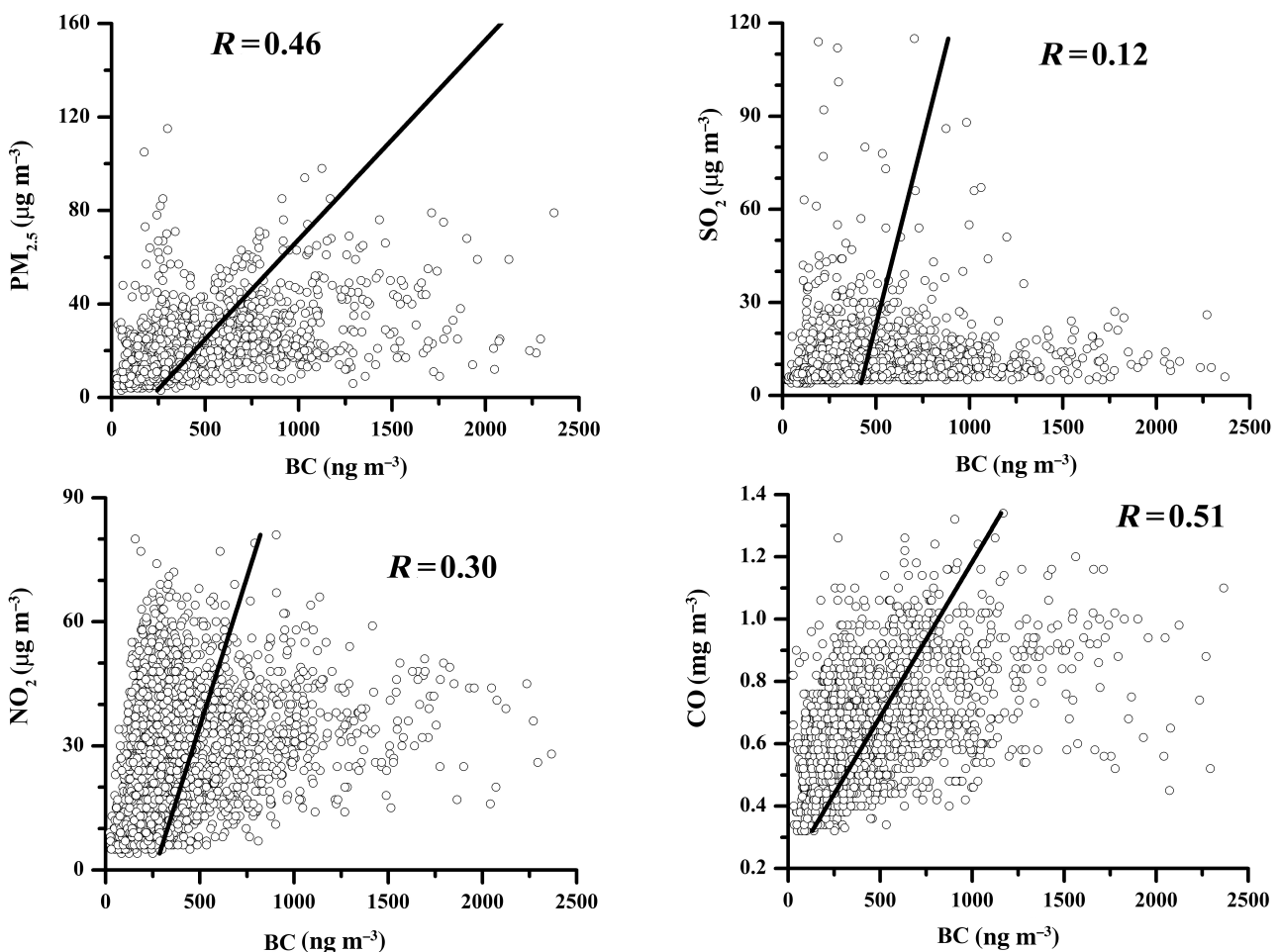


FIGURE 3 Correlation between black carbon and major pollutants during the observation period.

increased at 05:00, and its first peak appeared at 08:00. Afterward, the mass concentration decreased rapidly and reached the lowest value at 14:00–15:00, which indicated that traffic source emissions make the main contribution to the morning rush hour in BC. However, the evening peak of NO<sub>2</sub> occurs at 20:00, and the value of the evening peak is significantly larger than the value of the morning peak. In comparison, the mass concentration of the evening peak in BC is lower, only 55.2% of the morning peak, which shows that the traffic source emissions have a small contribution to the evening peak in BC. There is an apparent bimodal diurnal variation in CO, with peaks at 08:00 and 20:00, mainly from the incomplete combustion process and cooking emissions of carbonaceous substances. The diurnal change of CO is similar to BC; the mass concentration of the first (morning) peak is higher than that of the second (evening) peak, but the time of the evening peak lags behind that of BC. In addition, 08:00 is also the breakfast time for residents, so the impact of the morning peak of BC mass concentration is more complicated, mainly related to

traffic emissions, cooking emissions, and incomplete combustion of carbonaceous substances.

The BC's diurnal variation has a good anti-correlation with wind speed (Figure 6). At 08:00, the wind speed reached its minimum value, and BC reached the morning peak at this time; after that, the wind speed increased rapidly, and the BC mass concentration also quickly decreased. The wind speed remained high from 13:00 to 15:00 when BC reached the minimum value. After that, the wind speed decreased rapidly, and the BC mass concentration increased again. At 18:00, there was a valley in the visibility (Figure 6), corresponding to the evening peak in BC, which is mostly dinner time for residents. Therefore, the evening peak of BC may be caused by emissions from residential cooking sources under unfavorable meteorological conditions for dispersal.

In addition, Figure 5 shows that PM<sub>2.5</sub> and PM<sub>10</sub> have consistent diurnal variations, both of which are bimodal distributions, with peaks located at 10:00 and 22:00. The diurnal variation of O<sub>3</sub> is a unimodal distribution, with a peak at 15:00, which is similar to the diurnal variation of

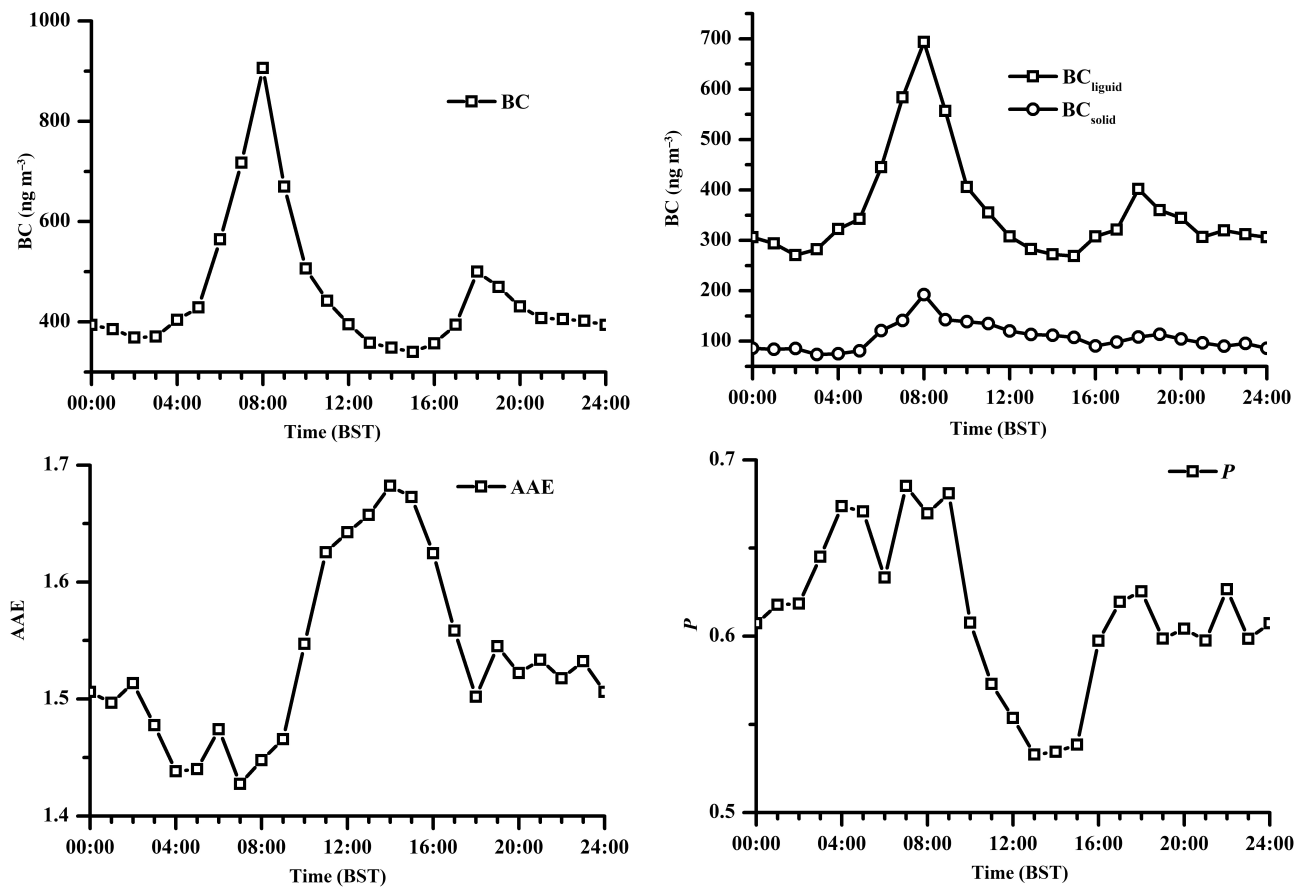


**FIGURE 4** Diurnal variation of black carbon (BC), BC<sub>liquid</sub>, BC<sub>solid</sub>, absorption Ångström exponent, and  $P$  during the observation period.

temperature. The diurnal temperature variation in Etuoke Banner is unimodal (Figure 6). The temperature increases rapidly after sunrise at 07:00, reaches the maximum value at 14:00–16:00, and then decreases rapidly. In the afternoon, the temperature is higher, the photochemical process is intense, and the O<sub>3</sub> generated reaches its peak. The diurnal variation of RH is opposite to that of temperature. After sunrise, it decreases rapidly, reaches the minimum value at 14:00–16:00, and increases quickly. Wind speed is a similar diurnal variation to temperature, with an apparent unimodal distribution, reaching its peak at 16:00. The temperature is lower, the wind speed is weaker, and the RH is higher during the morning peak. At this time, the height of ABL is lower, which is beneficial to the accumulation of ground atmospheric pollutants. Therefore, BC, PM, NO<sub>2</sub>, and CO all observed pronounced mass concentration peaks. During the evening peak, the wind speed is higher, the RH increases gradually, and the diffusion condition begins to weaken. However, it is still stronger than in the morning, which means that diffusion conditions are better than in the morning, which is not conducive to accumulating atmospheric pollutants, so BC, PM<sub>10</sub>, PM<sub>2.5</sub>, CO, and SO<sub>2</sub>

gradually decrease. The value of the evening peak is lower than that of the morning peak.

In summary, the diurnal variations in BC, PM<sub>2.5</sub>, PM<sub>10</sub>, NO<sub>2</sub>, SO<sub>2</sub>, and CO are mainly caused by the diurnal variations in anthropogenic emissions' intensity and meteorological conditions. ABL is stable at night. Although anthropogenic emissions emit fewer pollutants, the height of ABL, wind speed, and RH are lower, so atmospheric pollutants are easy to accumulate. After sunrise, the earth's surface is heated, and the stable ABL begins to destroy. However, the ground-level inversion layer still exists, and the wind speed is still low. When pollutants emitted by anthropogenic emissions such as cooking and traffic sources in the morning are superimposed, air pollutants' mass concentration peaks. Afterward, with the destruction of the stable ABL, a mixed layer is formed in ABL, and the high wind speed benefits the diffusion of atmospheric pollutants. Hence, the mass concentration of atmospheric pollutants decreases rapidly. In the afternoon, as solar radiation weakens, wind speed decreases, and stable ABL forms again. When the atmospheric pollutants emitted by anthropogenic emissions are superimposed during the evening rush hour,

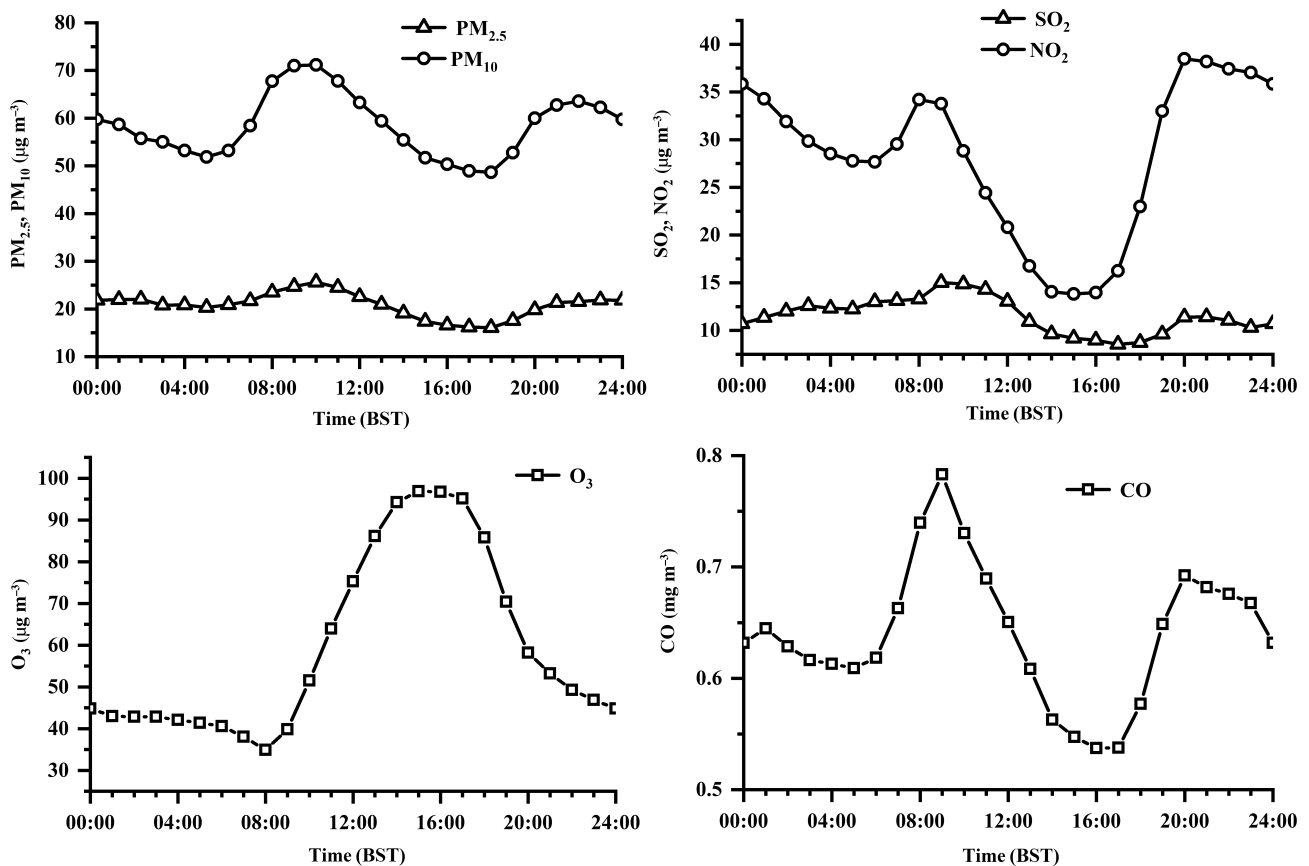


FIGURE 5 Diurnal variation of major atmospheric pollutants during the observation period.

the mass concentration of atmospheric pollutants will reach a second peak. However, there are differences in meteorological conditions and anthropogenic emissions intensity during the morning and evening peak periods, so there are differences in atmospheric pollutants' morning and evening peak values.

There is a noticeable unimodal diurnal variation in AAE, peaking at 14:00 (Figure 4). AAE's diurnal variation is more significant; it is lower at night, reaches the minimum value of 1.43 at 07:00, and is higher during the day, getting the maximum value of 1.68 at 14:00. At night, the RH is higher, the wind speed is lower, and the BC particles emitted into the atmosphere stay longer in the atmosphere and are prone to aging, so the particle size is relatively larger and the value of AAE is lower. In the daytime, there are more human activities, more BC particles are directly emitted, and the particle size of BC particles is smaller. In addition, there is a high temperature and low RH in the daytime, which is not beneficial to the aging of BC particles, so most BC particles are in a fresh state with a small particle size. The diurnal variation of  $P$  is also considerable, and the  $P$  value can reach 0.69 at 08:00. Still, only 0.53 at 13:00. The peak time of  $P$  coincides with that of BC, which confirms that the

traffic emission has a more significant contribution to BC. The diurnal variation of BC<sub>liquid</sub> and BC<sub>solid</sub> are both bimodal distributions, consistent with the diurnal variation of BC. In addition, Figure 4 shows that  $P$  also has a growth trend in 02:00–04:00, but the mass concentration of BC is very low. Figure 6 shows that the wind speed increases slightly from 02:00 to 04:00. Ordos City is a vital coal production base in China, and there are many transport trucks at night. Therefore, the change in  $P$  value between 02:00 and 04:00 may be due to the transmission of atmospheric pollutants emitted by transport vehicles at night.

### 3.3 | Distribution characteristics of air pollutants under different BC mass concentrations

The mass concentration range of BC is 0–700  $\text{ng m}^{-3}$  in Etuoke Banner (Figure 7), which can account for 86.0% of the total observation period, and the highest probability in the range of 100–300  $\text{ng m}^{-3}$ , which can account for 34.12%. With the increased BC, the wind speed decreased and then increased. When the BC's mass

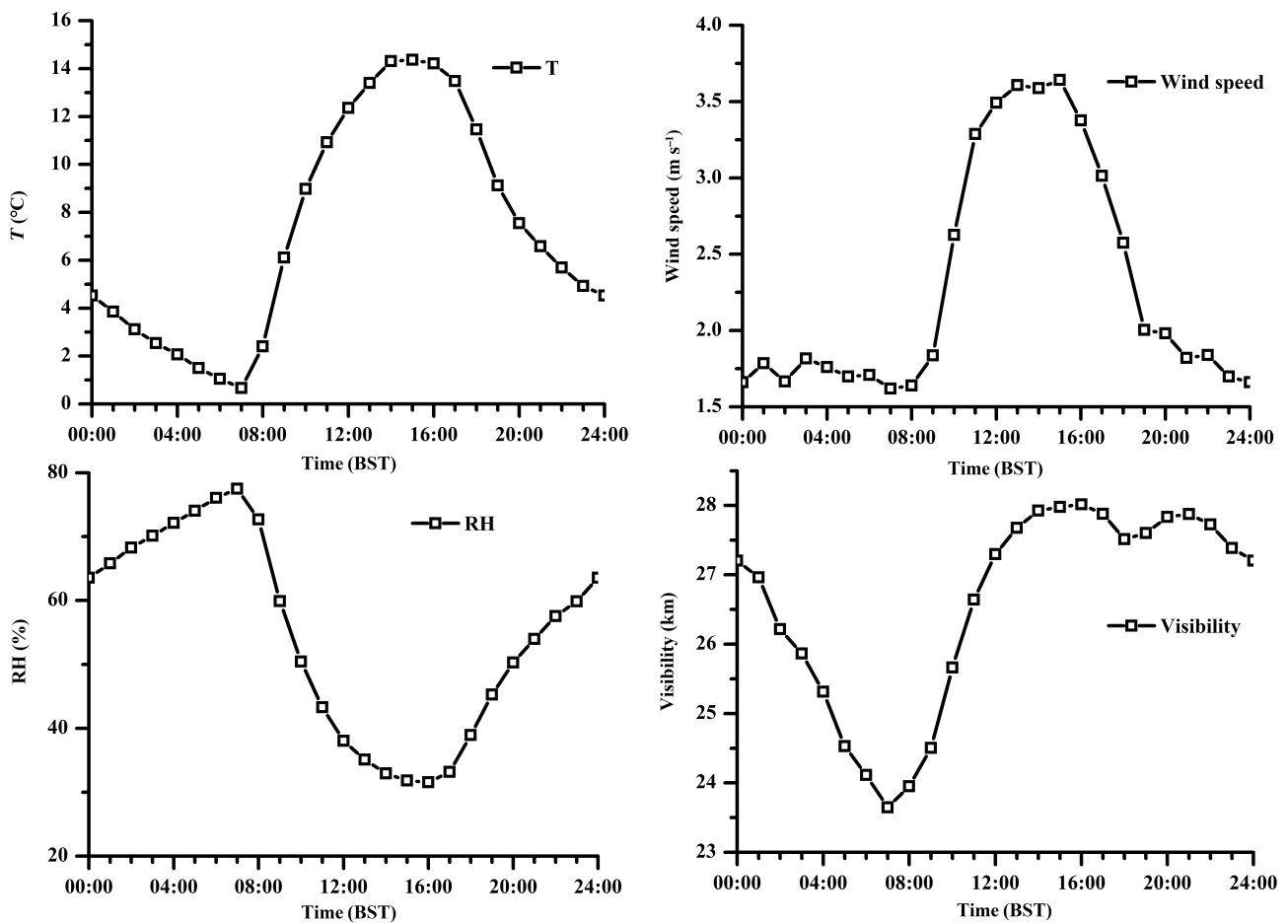


FIGURE 6 Diurnal variation of meteorological elements during the observation period.

concentration is  $0\text{--}1700 \text{ ng m}^{-3}$ , wind speed gradually decreases with the increase of BC. When the BC's mass concentration is  $0\text{--}100 \text{ ng m}^{-3}$ , the maximum value of wind speed can reach  $3.0 \text{ m s}^{-1}$ , and when the BC's mass concentration is  $1500\text{--}1700 \text{ ng m}^{-3}$ , the minimum value of wind speed is only  $1.1 \text{ m s}^{-1}$ . The higher wind speed can benefit the diffusion of atmospheric pollutants, so BC has a lower mass concentration. However, wind speed gradually increases with the increase of BC in  $1700\text{--}2400 \text{ ng m}^{-3}$ . Still, the change of wind speed is small at this time, ranging from  $1.1$  to  $1.6 \text{ m s}^{-1}$  (Figure 7). Overall, the wind speed is small, and the horizontal diffusion is weak during the high mass concentration of BC.

The value of AAE decreased with the increase in BC, and the maximum value of AAE was 1.7 when the BC was  $0\text{--}100 \text{ ng m}^{-3}$ . The BC's residence time is shorter in the atmosphere when wind speed is higher, so the aging degree of BC is weaker (Forbes et al., 2006; Tan et al., 2022), resulting in a larger value of AAE when the mass concentration of BC is smaller. Studies have shown that when the AAE value is approximately equal to 1, BC is dominated by traffic sources (liquid fuels); when AAE

is roughly equivalent to 2, it indicates that BC mainly comes from biomass combustion (Martinsson et al., 2015). This shows that with the increase in BC, the biomass-burning combustion process contributed to decreases, and the traffic source emission contributed to increases. The *P* value gradually decreases with the increase in BC, indicating that the proportion of  $\text{BC}_{\text{liquid}}$  gradually increases, that is, the contribution of traffic sources increases (Figure 7). In addition, the smaller the value of AAE, the larger the size of aerosol (Drinovec et al., 2015; Wang et al., 2020). This indicates that the aerosol particle size is larger, and the degree of aging is higher when BC is higher in Etouke Banner. RH increases with the increase in BC (Figure 7). The wind speed is low, and the RH is large when BC's mass concentration is high, which is also suitable for BC aging. Particle size increases, enhancing the extinction characteristics of aerosol particles, so the visibility also decreases with the increase in BC.

The PM also increases with the increase in BC's mass concentration. The varied range of  $\text{PM}_{2.5}$  is higher than that of  $\text{PM}_{10}$  (Figure 8).  $\text{PM}_{2.5}$  and  $\text{PM}_{10}$  were the lowest

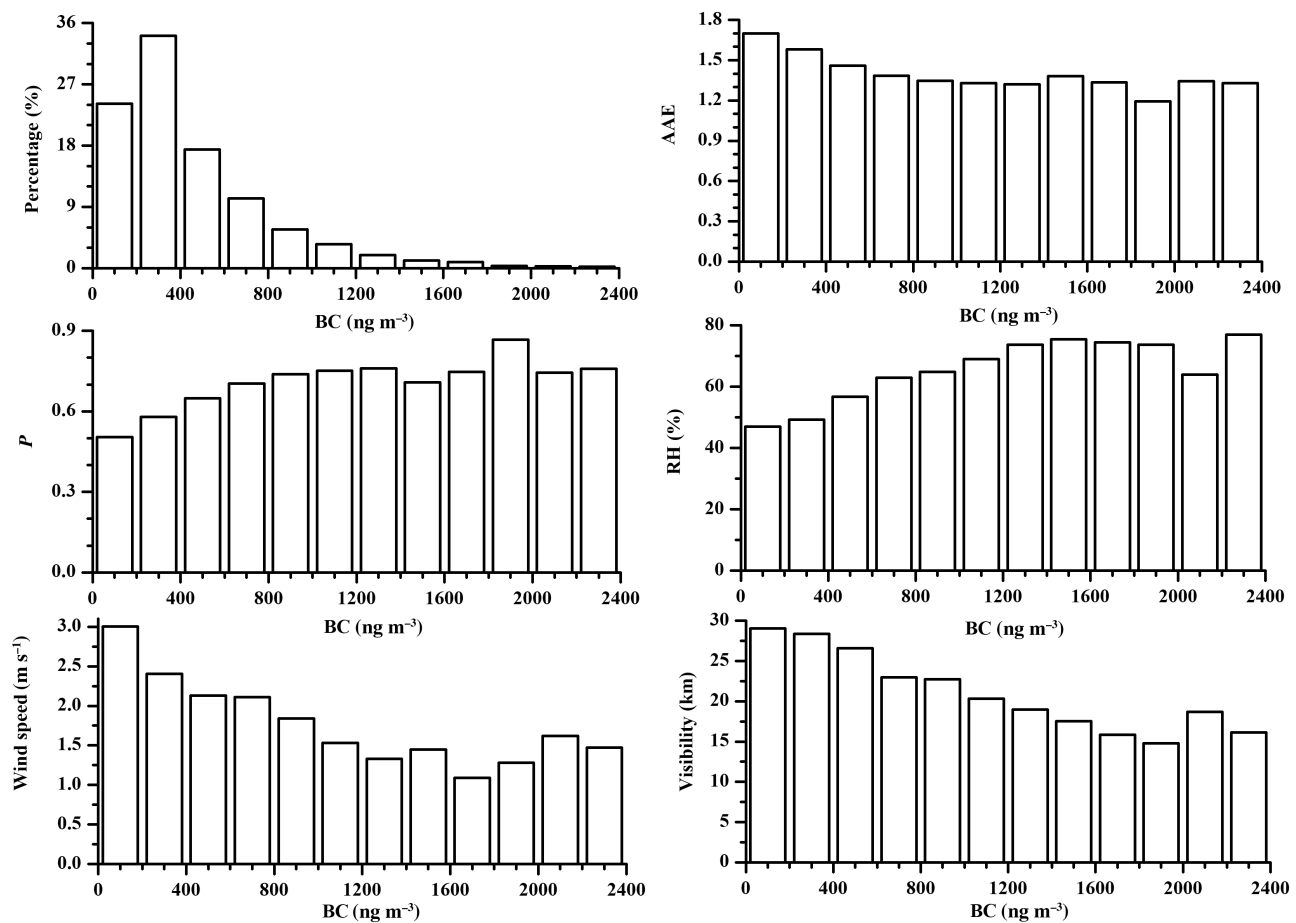


**FIGURE 7** Percentage occurrences of black carbon and the corresponding variations of absorption Ångström exponent,  $P$ , and meteorological elements.

when BC in  $0\text{--}100 \text{ ng m}^{-3}$ , which were 13.5 and  $47.7 \mu\text{g m}^{-3}$ , respectively. PM<sub>2.5</sub> and PM<sub>10</sub> were the highest when BC is in the range  $1700\text{--}1900 \text{ ng m}^{-3}$ , 39.5 and  $85.0 \mu\text{g m}^{-3}$ , respectively. CO and NO<sub>2</sub> also increased with the increase in BC's mass concentration. CO and NO<sub>2</sub> mainly come from the incomplete combustion of carbonaceous materials and traffic source emissions, respectively (Li et al., 2021; Shen, Wang, Kong, Zhang, et al., 2021). The two emissions have good homology with BC's, so CO and NO<sub>2</sub> also increase when BC increases. SO<sub>2</sub> varies little in different BC's mass concentration intervals (Figure 8). SO<sub>2</sub> mostly comes from industrial coal-burning emissions (Pei et al., 2022). This shows that the contribution of coal-burning sources under different BC mass concentrations in Etuoke Banner is relatively stable. O<sub>3</sub> decreases with the increase in BC's mass concentration. Photochemical processes primarily generate O<sub>3</sub>, and the high value of O<sub>3</sub> usually occurs in the afternoon (14:00–16:00). When the mass concentration of O<sub>3</sub> is higher, the temperature, the height of ABL, and wind speed are higher (Figure 6), and the atmospheric diffusion conditions are better, which is conducive to the

spread of BC. BC has a higher mass concentration in the morning or night during the observation period (Figure 4). At this time, the photochemical process generates less O<sub>3</sub>, and due to the titration of NO emitted by traffic source emissions, the mass concentration of O<sub>3</sub> is lower. Therefore, O<sub>3</sub> decreases with the increase of BC.

### 3.4 | The potential source area and potential affecting area analysis

The value of PSCF ranges from 0 to 1. The larger the PSCF value, the greater the grid area's impact on the target point's pollutant concentration (Lucey et al., 2001). Figure 9 shows that PM<sub>2.5</sub> and BC high PSCF value areas are mainly located around Etuoke Banner, and the PSCF value exceeds 0.8, which shows that even in grassland areas, PM<sub>2.5</sub> and BC mainly come from local source emissions. It can be found that PM<sub>2.5</sub> potential source areas in Etuoke Banner mainly come from two regions (Figure 9): Shizuishan City–Yinchuan City–Alxa League in the west and Etuoqeqian Banner–Wuzhong

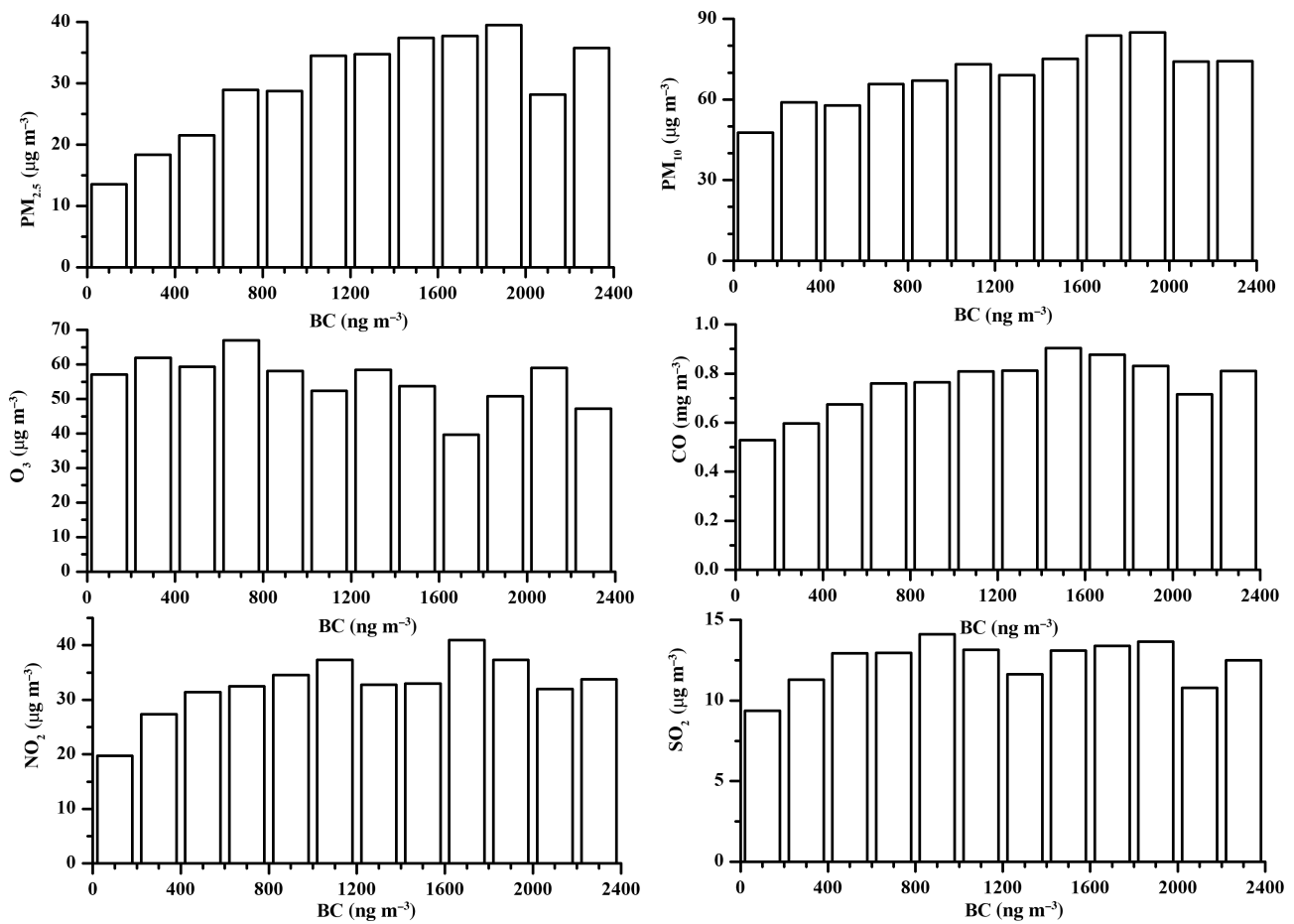


**FIGURE 8** The corresponding variations of major atmospheric pollutants under different black carbon mass concentrations.

City–Qingyang City in the north. The PSCF values of the areas are all 0.7–0.8. The potential sources of BC also mainly come from these two areas, but the PSCF values of Shizuishan City–Yinchuan City–Alxa League in the west are lower, mostly 0.6–0.7; the PSCF values of Etuoqian Banner–Wuzhong City–Qingyang City in the north are higher, mostly 0.7–0.8.

Unlike the PSCF model, the CWT model could give the quantitative contribution of potential source areas. Figure 9 indicates that the spatial distribution of the PM<sub>2.5</sub> and BC high CWT value areas is similar to that of PSCF. The PM<sub>2.5</sub> high CWT value areas are mainly located around Etuoqian Banner, and their contribution to PM<sub>2.5</sub> exceeds 18  $\mu\text{g m}^{-3}$ . The grassland resource area of Etuoqian Banner is 19,710 km<sup>2</sup> accounting for 94% of the total land area. The population in 2022 is only 168,000, but the raw coal output of the entire banner is 45.125 million tons. The Etuoqian Banner has fewer anthropogenic source emissions and better air quality. In 2022, the ambient air quality in Etuoqian Banner (Wulan Town) was excellent for 323 days throughout the year, and there were 24 polluted days. The proportion of days with excellent ambient air was 93.1%. The annual average mass

concentrations of SO<sub>2</sub>, NO<sub>2</sub>, and PM<sub>2.5</sub> were 14, 15, and 21  $\mu\text{g m}^{-3}$ , respectively ([http://www.eq.gov.cn/eqxxgk/gkml/qq\\_etkq\\_5241/qq\\_etkq\\_0402/202307/t20230705\\_3446929.html](http://www.eq.gov.cn/eqxxgk/gkml/qq_etkq_5241/qq_etkq_0402/202307/t20230705_3446929.html)). However, biomass straw burning, open-pit coal mining, and industrial sources in the Ordos region contribute significantly to PM<sub>2.5</sub> and carbonaceous components (Cheng et al., 2007; Khuzestani et al., 2018; Li et al., 2021; Zhang et al., 2010). The Alxa League–Yinchuan City and Etuoqian Banner areas have the second most significant contribution to PM<sub>2.5</sub> and contribute 12–18  $\mu\text{g m}^{-3}$  to PM<sub>2.5</sub>. There are still some long-distance transports of PM<sub>2.5</sub> (Figure 9), such as Lanzhou, Xining, Xi'an, and Zhengzhou, but the CWT values are low, mostly 2–4  $\mu\text{g m}^{-3}$ . BC's high CWT value area is also mainly located in Etuoqian Banner (Figure 9), with high CWT values' contribution exceeding 500 ng m<sup>-3</sup>. Etuoqian Banner–Wuzhong City–Qingyang City in the north has high CWT values (300–500 ng m<sup>-3</sup>), and the Shizuishan City–Yinchuan City–Alxa League area in the west has high CWT values (200–400 ng m<sup>-3</sup>). Unlike PM<sub>2.5</sub>, the BC has almost no long-distance transportation.

Figure 10 shows that the PM<sub>2.5</sub> and BC of forward trajectory PSCF spatial distributions are similar.

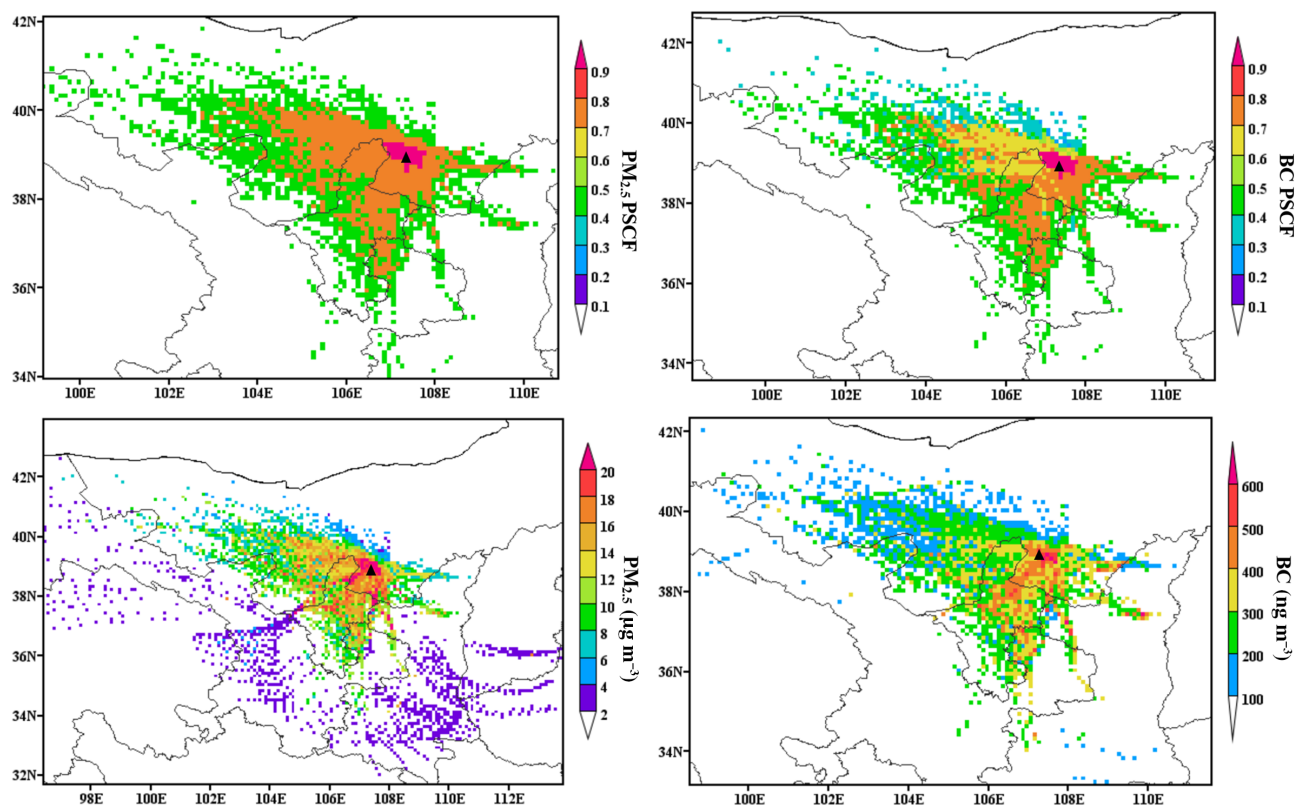


**FIGURE 9** Backward trajectories of PM<sub>2.5</sub> and black carbon by potential source contribution function and concentration-weighted trajectory models.

The high-value areas are mainly concentrated in the east of Etuoke Banner, where Etuoke Banner and Wushen Banner have the highest PSCF values exceeding 0.8; the PSCF value in the Wuhai City–Ordos City–Shenmu City–Yulin City area is 0.7–0.8. In addition, there is a long and narrow transmission belt in Yulin City–Lüliang City–Changzhi City (Figure 10), with a PSCF value of 0.4–0.8. Overall, after 48 h of transmission, PM<sub>2.5</sub> and BC in Etuoke Banner mainly affect its surrounding areas. This is followed by a more significant impact on northern Shaanxi and western Shanxi provinces and can be transmitted as far as Hebei and Beijing.

Figure 10 shows that the spatial distribution of PM<sub>2.5</sub> and BC CWT high-value potential affecting areas is similar, mainly concentrated in the Etuoke Banner areas, Etuoke Banner–Hangjin Banner–Etuokekian Banner–Wushen Banner areas with CWT values of PM<sub>2.5</sub> and BC exceeding 12 and 400 ng m<sup>-3</sup>, respectively. The Shenmu City–Yulin City–Shuozhou City–Lüliang City area has low PM<sub>2.5</sub> and BC CWT values being 6–12 µg m<sup>-3</sup> and 100–400 ng m<sup>-3</sup>, respectively. PM<sub>2.5</sub> and BC could be transported over long distances after 48 h (Figure 10), affecting areas such as Mongolia, Hebei province, and Beijing. The spatial range of long-distance transport of PM<sub>2.5</sub> is more significant than that of BC.

## 4 | CONCLUSIONS

To obtain the characteristics of BC in the typical grassland environment in China, continuous observations of BC were carried out in Etuoke Banner, a typical grassland environment in Ordos, from September 8 to December 1, 2022. BC in Etuoke Banner in autumn is 22.4–4667.5 ng m<sup>-3</sup>, and the average concentration is 456.6 ng m<sup>-3</sup>, accounting for 2.20% of the mass fraction of PM<sub>2.5</sub>. BC<sub>liquid</sub> is the main component of BC (accounting for 79.2%); the average concentration is 361.7 ng m<sup>-3</sup>. The average values of PM<sub>10</sub>, PM<sub>2.5</sub>, NO<sub>2</sub>, O<sub>3</sub>, SO<sub>2</sub>, and CO are 58.4, 20.8, 27.9, 59.8, 11.6 µg m<sup>-3</sup>, and 0.64 mg m<sup>-3</sup>. The primary sources of BC emissions in Etuoke Banner are combustion processes and traffic emissions, with little industrial emission contribution. The diurnal variations of BC, BC<sub>liquid</sub>, and BC<sub>solid</sub> are bimodal, with peaks at 08:00 and 18:00. The first peak (morning peak) is mainly related to traffic sources, cooking sources, and incomplete combustion of carbon-containing substances; the second peak (evening peak) may be caused by emissions from residential cooking sources under the influence of meteorological conditions that are not beneficial to diffusion. The diurnal variation of AAE is unimodal, with the peak at 14:00. With the

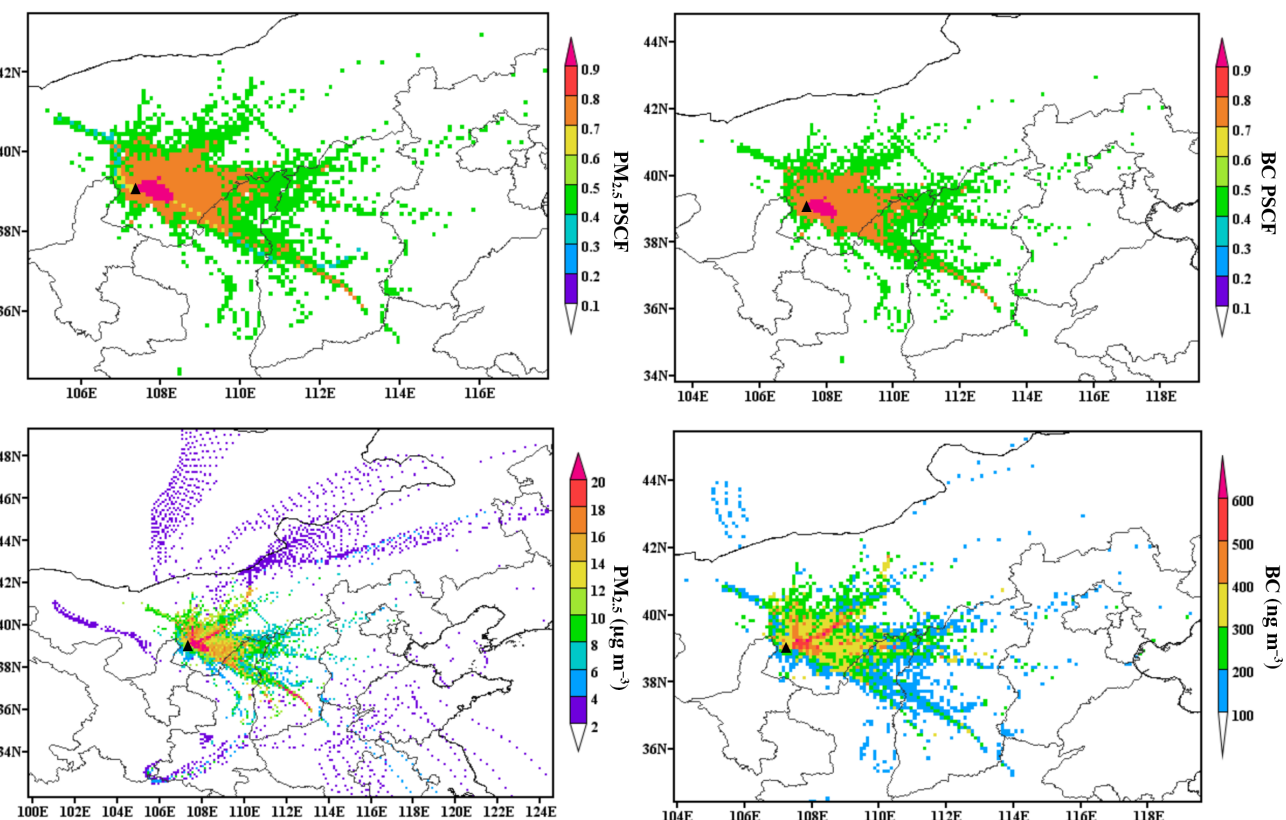


**FIGURE 10** Forward trajectories of  $\text{PM}_{2.5}$  and black carbon by potential source contribution function and concentration-weighted trajectory models.

increase in BC mass concentration, AAE and visibility gradually decreased, wind speed first decreased and then increased,  $P$  and RH gradually increased, and the biomass combustion sources contributing to BC decreased. In contrast, traffic sources contribute to BC's increase. The evolution characteristics of atmospheric pollutants differed with the increase in BC concentration. PM, CO, and  $\text{NO}_2$  increased with BC, and the variation of  $\text{PM}_{2.5}$  concentration was higher than that of  $\text{PM}_{10}$ . The mass concentration of  $\text{SO}_2$  varies little in different BC concentration intervals, which shows that the contribution of coal-burning sources under different BC mass concentrations in Etuoke Banner is relatively stable. The mass concentration of  $\text{O}_3$  decreases with increase in the BC. The potential sources and affecting areas of BC and  $\text{PM}_{2.5}$  are mainly concentrated around Etuoke Banner and can affect the NCP region after 48 h of transmission.

## AUTHOR CONTRIBUTIONS

**Yanhong Li:** Conceptualization (equal); data curation (equal); resources (equal); software (equal); supervision (equal); validation (equal); writing – original draft (equal). **Jinwen Zhang:** Data curation (equal); software (equal); validation (equal). **Qiyong Duan:** Data curation (equal); methodology (equal); writing – original draft (equal). **Xiangchen Kong:** Investigation (equal);

methodology (equal); software (equal). **Honglei Wang:** Methodology (equal); supervision (equal); validation (equal); writing – review and editing (equal).

## ACKNOWLEDGEMENTS

This work was supported by the National Natural Science Foundation of China (Grant Nos. 42275196 and 41830965), the Natural Science Foundation of Jiangsu Province (Grant No. BK20231300), and Wuxi University Research Start-up Fund for Introduced Talents (Grant No. 2023r035). Open fund by Jiangsu Key Laboratory of Atmospheric Environment Monitoring and Pollution Control (Grant Nos. KHK2207).

## DATA AVAILABILITY STATEMENT

The data that support the findings of this study are available from the corresponding author upon reasonable request.

## ORCID

Honglei Wang  <https://orcid.org/0000-0001-5535-6651>

## REFERENCES

- Aruna, K., Kumar, T.L., Rao, D.N., Murthy, B.K., Babu, S.S. & Moorthy, K.K. (2013) Black carbon aerosols in a tropical semi-urban coastal environment: effects of boundary layer dynamics

- and long range transport. *Journal of Atmospheric and Solar-Terrestrial Physics*, 104, 116–125.
- Atamny, F., Blöcker, J., Dübotzky, A., Kurt, H., Timpe, O., Loose, G. et al. (1992) Surface chemistry of carbon: activation of molecular oxygen. *Molecular Physics*, 76(4), 851–886.
- Chen, D., Zhao, W., Zhang, L., Zhao, Q., Zhang, J., Chen, F. et al. (2023) Characterization and source apportionment for light absorption amplification of black carbon at an urban site in eastern China. *Science of the Total Environment*, 865, 161180.
- Chen, W., Cao, X., Ran, H., Chen, T., Yang, B. & Zheng, X. (2022) Concentration and source allocation of black carbon by AE-33 model in urban area of Shenzhen, southern China. *Journal of Environmental Health Science & Engineering*, 20(1), 469–483.
- Chen, Y.W., Cheng, Y.H. & Hsu, C.Y. (2023) Characterization of the sources and health risks of polycyclic aromatic hydrocarbons in PM<sub>2.5</sub> and their relationship with black carbon: a case study in northern Taiwan. *Environmental Pollution*, 336, 122427.
- Cheng, X., An, S., Chen, J., Li, B., Liu, Y. & Liu, S. (2007) Spatial relationships among species, above-ground biomass, N, and P in degraded grasslands in Ordos Plateau, northwestern China. *Journal of Arid Environments*, 68(4), 652–667.
- Chung, S.H. & Seinfeld, J.H. (2005) Climate response of direct radiative forcing of anthropogenic black carbon. *Journal of Geophysical Research*, 110(D11), D11102. Available from: <https://doi.org/10.1029/2004JD005441>
- Ding, A.J., Huang, X., Nie, W., Sun, J.N., Kerminen, V.M., Petäjä, T. et al. (2016) Enhanced haze pollution by black carbon in megacities in China. *Geophysical Research Letters*, 43(6), 2873–2879.
- Drinovec, L., Močnik, G., Zotter, P., Prévôt, A.S.H., Ruckstuhl, C., Coz, E. et al. (2015) The "dual-spot" Aethalometer: an improved measurement of aerosol black carbon with real-time loading compensation. *Atmospheric Measurement Techniques*, 8(5), 1965–1979.
- Emerson, E.W., Katich, J.M., Schwarz, J.P., McMeeking, G.R. & Farmer, D.K. (2018) Direct measurements of dry and wet deposition of black carbon over a grassland. *Journal of Geophysical Research: Atmospheres*, 123(21), 12277–12290.
- Forbes, M.S., Raison, R.J. & Skjemstad, J.O. (2006) Formation, transformation and transport of black carbon (charcoal) in terrestrial and aquatic ecosystems. *Science of the Total Environment*, 370(1), 190–206.
- Friedman, C., Dabelea, D., Glueck, D.H., Allshouse, W.B., Adgate, J.L., Keller, K.P. et al. (2023) Early-life exposure to residential black carbon and childhood cardiometabolic health. *Environmental Research*, 10, 117285.
- Gao, C., Xing, C., Tan, W., Lin, H., Bu, N., Xue, J. et al. (2023) Vertical characteristics and potential sources of aerosols over Northeast China using ground-based MAX-DOAS. *Atmospheric Pollution Research*, 14(3), 101691.
- Gramsch, E., Muñoz, A., Langner, J., Morales, L., Soto, C., Pérez, P. et al. (2020) Black carbon transport between Santiago de Chile and glaciers in the Andes Mountains. *Atmospheric Environment*, 232, 117546.
- Gu, Y., Zhang, W., Yang, Y., Wang, C., Streets, D.G. & Yim, S.H.L. (2020) Assessing outdoor air quality and public health impact attributable to residential black carbon emissions in rural China. *Resources, Conservation & Recycling*, 159, 104812.
- Hao, W.M., Petkov, A., Nordgren, B.L., Corley, R.E., Silverstein, R.P., Urbanski, S.P. et al. (2016) Daily black carbon emissions from fires in northern Eurasia for 2002–2015. *Geoscientific Model Development*, 9(12), 4461–4474.
- Hirdman, D., Burkhardt, J.F., Sodemann, H., Eckhardt, S., Jefferson, A., Quinn, P.K. et al. (2010) Long-term trends of black carbon and sulphate aerosol in the Arctic: changes in atmospheric transport and source region emissions. *Atmospheric Chemistry and Physics*, 10(19), 9351–9368.
- Kant, Y., Natwariya, A., Mitra, D. & Chauhan, P. (2023) Impact of vegetation fires on regional aerosol black carbon over south and east Asia. In: *Vegetation fires and pollution in Asia*. Cham: Springer International Publishing, pp. 465–481.
- Khuzestani, R.B., Schauer, J.J., Shang, J., Cai, T., Fang, D., Wei, Y. et al. (2018) Source apportionments of PM<sub>2.5</sub> organic carbon during the elevated pollution episodes in the Ordos region, Inner Mongolia, China. *Environmental Science and Pollution Research*, 25, 13159–13172.
- Lei, S., Ge, B., Liu, H., Quan, J., Xu, D., Zhang, Y. et al. (2023) Refractory black carbon aerosols in rainwater in the summer of 2019 in Beijing: mass concentration, size distribution and wet scavenging ratio. *Journal of Environmental Sciences*, 132, 31–42.
- Li, A., Chen, C., Chen, J. & Lei, P. (2021) Environmental investigation of pollutants in coal mine operation and waste dump area monitored in Ordos region, China. *RSC Advances*, 11(17), 10340–10352.
- Li, Y., Henze, D.K., Jack, D., Henderson, B.H. & Kinney, P.L. (2016) Assessing public health burden associated with exposure to ambient black carbon in the United States. *Science of the Total Environment*, 539, 515–525.
- Li, Z., Guo, J., Ding, A., Liao, H., Liu, J., Sun, Y. et al. (2017) Aerosol and boundary-layer interactions and impact on air quality. *National Science Review*, 4(6), 810–833.
- Liakakou, E., Stavroulas, I., Kaskaoutis, D.G., Grivas, G., Paraskevopoulou, D., Dumka, U.C. et al. (2020) Long-term variability, source apportionment and spectral properties of black carbon at an urban background site in Athens, Greece. *Atmospheric Environment*, 222, 117137.
- Lim, S., Lee, M. & Yoo, H.J. (2023) Size distributions, mixing state, and morphology of refractory black carbon in an urban atmosphere of Northeast Asia during summer. *Science of the Total Environment*, 856, 158436.
- Lin, W., Dai, J., Liu, R., Zhai, Y., Yue, D. & Hu, Q. (2019) Integrated assessment of health risk and climate effects of black carbon in the Pearl River Delta region, China. *Environmental Research*, 176, 108522.
- Liu, X., Wang, S., Zhang, Q., Jiang, C., Liang, L., Tang, S. et al. (2023) Origins of black carbon from anthropogenic emissions and open biomass burning transported to Xishuangbanna, Southwest China. *Journal of Environmental Sciences*, 125, 277–289.
- Liu, Y., Yan, C. & Zheng, M. (2018) Source apportionment of black carbon during winter in Beijing. *Science of the Total Environment*, 618, 531–541.
- Lu, W., Zhu, B., Liu, X., Dai, M., Shi, S., Gao, J. et al. (2023) The influence of regional transport on the three-dimensional distributions of black carbon and its sources over eastern China. *Atmospheric Environment*, 297, 119585.

- Lucey, D., Hadjiiski, L., Hopke, P.K., Scudlark, J.R. & Church, T. (2001) Identification of sources of pollutants in precipitation measured at the mid-Atlantic US coast using potential source contribution function (PSCF). *Atmospheric Environment*, 35(23), 3979–3986.
- Martinsson, J., Eriksson, A.C., Nielsen, I.E., Malmborg, V.B., Ahlberg, E., Andersen, C. et al. (2015) Impacts of combustion conditions and photochemical processing on the light absorption of biomass combustion aerosol. *Environmental Science & Technology*, 49(24), 14663–14671.
- Ni, M., Huang, J., Lu, S., Li, X., Yan, J. & Cen, K. (2014) A review on black carbon emissions, worldwide and in China. *Chemosphere*, 107, 83–93.
- Ozdemir, H., Pozzoli, L., Kindap, T., Demir, G., Mertoglu, B., Mihalopoulos, N. et al. (2014) Spatial and temporal analysis of black carbon aerosols in Istanbul megacity. *Science of the Total Environment*, 473, 451–458.
- Pani, S.K., Wang, S.H., Lin, N.H., Chantara, S., Lee, C.T. & Thepnuan, D. (2020) Black carbon over an urban atmosphere in northern peninsular Southeast Asia: characteristics, source apportionment, and associated health risks. *Environmental Pollution*, 259, 113871.
- Park, S.U. & Park, M.S. (2014) Aerosol size distributions observed at Naiman in the Asian dust source region of Inner Mongolia. *Atmospheric Environment*, 82, 17–23.
- Pei, Y., Wang, H., Tan, Y., Zhu, B., Zhao, T., Lu, W. et al. (2022) Analysis of BC pollution characteristics under PM<sub>2.5</sub> and O<sub>3</sub> pollution conditions in Nanjing from 2015 to 2020. *Atmosphere*, 13(9), 1440.
- Rodionov, A., Amelung, W., Peinemann, N., Haumaier, L., Zhang, X., Kleber, M. et al. (2010) Black carbon in grassland ecosystems of the world. *Global Biogeochemical Cycles*, 24(3), GB3013. Available from: <https://doi.org/10.1029/2009GB003669>
- Roostaei, V., Faridi, S., Momeniha, F., Yousefian, F., Mokammel, A., Niazi, S. et al. (2023) Black carbon temporal trends and associated health and economic impacts in Tehran. *Atmospheric Pollution Research*, 6, 101815.
- Rosa, M.J., Yan, B., Chillrud, S.N., Acosta, L.M., Divjan, A., Jacobson, J.S. et al. (2014) Domestic airborne black carbon levels and 8-isoprostane in exhaled breath condensate among children in New York City. *Environmental Research*, 135, 105–110.
- Safai D., Kewat, S., Praveen S., Rao S.P., Momin, G.A., Ali, K. et al. (2007) Seasonal variation of black carbon aerosols over a tropical urban city of Pune, India. *Atmospheric Environment*, 41(13), 2699–2709.
- Schleicher, N., Norra, S., Fricker, M., Kaminski, U., Chen, Y., Chai, F. et al. (2013) Spatio-temporal variations of black carbon concentrations in the Megacity Beijing. *Environmental Pollution*, 182, 392–401.
- Shen, L., Wang, H., Kong, X., Yin, Y., Chen, K. & Chen, J. (2021) Characterization of black carbon aerosol at the summit of Mount Tai (1534 m) in central East China: temporal variation, source apportionment and transport. *Atmospheric Environment*, 246, 118152.
- Shen, L., Wang, H., Kong, X., Zhang, C., Shi, S. & Zhu, B. (2021) Characterization of black carbon aerosol in the Yangtze River Delta, China: seasonal variation and source apportionment. *Atmospheric Pollution Research*, 12(1), 195–209.
- Shores, C.A., Klapmeyer, M.E., Quadros, M.E. & Marr, L.C. (2013) Sources and transport of black carbon at the California-Mexico border. *Atmospheric Environment*, 70, 490–499.
- Shrestha, G., Traina, S.J. & Swanston, C.W. (2010) Black carbon's properties and role in the environment: a comprehensive review. *Sustainability*, 2(1), 294–320.
- Slater, J., Coe, H., McFiggans, G., Tonttila, J. & Romakkaniemi, S. (2022) The effect of BC on aerosol-boundary layer feedback: potential implications for urban pollution episodes. *Atmospheric Chemistry and Physics*, 22(4), 2937–2953.
- Talukdar, S. & Ratnam, M.V. (2023) Mutual response hypothesis between surface temperature and aerosol (BC and non-BC) mass concentration observed in an urban environment. *Science of the Total Environment*, 887, 164048.
- Tan, S.C., Shi, G.Y. & Wang, H. (2012) Long-range transport of spring dust storms in Inner Mongolia and impact on the China seas. *Atmospheric Environment*, 46, 299–308.
- Tan, Y., Wang, H., Shi, S., Shen, L., Zhang, C., Zhu, B. et al. (2020) Annual variations of black carbon over the Yangtze River Delta from 2015 to 2018. *Journal of Environmental Sciences*, 96, 72–84.
- Tan, Y., Wang, H., Zhu, B., Zhao, T., Shi, S., Liu, A. et al. (2022) The interaction between black carbon and planetary boundary layer in the Yangtze River Delta from 2015 to 2020: why O<sub>3</sub> didn't decline so significantly as PM<sub>2.5</sub>. *Environmental Research*, 214, 114095.
- Tripathi, S.N., Dey, S., Tare, V. & Satheesh, S.K. (2005) Aerosol black carbon radiative forcing at an industrial city in northern India. *Geophysical Research Letters*, 32(8), L08802. Available from: <https://doi.org/10.1029/2005GL022515>
- Ulevicius, V., Byčenkienė, S., Bozzetti, C., VLACHOU, A., Plauškaitė, K., Mordas, G. et al. (2016) Fossil and non-fossil source contributions to atmospheric carbonaceous aerosols during extreme spring grassland fires in Eastern Europe. *Atmospheric Chemistry and Physics*, 16(9), 5513–5529.
- Venkatachari, P., Zhou, L., Hopke, P.K., Felton, D., Rattigan, O.V., Schwab, J.J. et al. (2006) Spatial and temporal variability of black carbon in New York City. *Journal of Geophysical Research*, 111(D10), D10S05. Available from: <https://doi.org/10.1029/2005JD006314>
- Wan, D., Han, Y., Song, L., Ning, D. & Jiang, Q. (2023) Sediment records of black carbon variations over the last two centuries in North China. *Science of the Total Environment*, 888, 164189.
- Wang, H., Ke, Y., Tan, Y., Zhu, B., Zhao, T. & Yin, Y. (2023) Observational evidence for the dual roles of BC in the megacity of eastern China: enhanced O<sub>3</sub> and decreased PM<sub>2.5</sub> pollution. *Chemosphere*, 327, 138548.
- Wang, H., Liu, S., Zhao, T., Lu, W., Xia, J. & Shi, S. (2023) Characteristics and source apportionment of black carbon over the eastern Tibetan Plateau. *Environmental Sciences*, 44(5), 2450–2460 (in Chinese).
- Wang, Q., Liu, H., Ye, J., Tian, J., Zhang, T., Zhang, Y. et al. (2020) Estimating absorption Ångström exponent of black carbon aerosol by coupling multiwavelength absorption with chemical composition. *Environmental Science & Technology Letters*, 8(2), 121–127.

- Wei, J., Huang, X.F., Peng, Y., Lin, X.Y., Lei, Z.H., Cao, L.M. et al. (2023) Evolution characteristic of atmospheric black carbon particles at a coastal site in the Pearl River Delta, China. *Environmental Pollution*, 324, 121380.
- Xie, F., Guo, L., Wang, Z., Tian, Y., Yue, C., Zhou, X. et al. (2023) Geochemical characteristics and socioeconomic associations of carbonaceous aerosols in coal-fueled cities with significant seasonal pollution pattern. *Environment International*, 179, 108179.
- Xin, J., Ma, Y., Zhao, D., Gong, C., Ren, X., Tang, G. et al. (2023) The feedback effects of aerosols from different sources on the urban boundary layer in Beijing China. *Environmental Pollution*, 325, 121440.
- Xu, H., Cheng, T., Gu, X., Yu, T., Xie, D. & Zheng, F. (2015) Spatio-temporal variability in dust observed over the Sinkiang and Inner Mongolia regions of northern China. *Atmospheric Pollution Research*, 6(4), 562–571.
- Yang, Z., Ma, N., Wang, Q., Li, G., Pan, X., Dong, W. et al. (2022) Characteristics and source apportionment of black carbon aerosol in the North China plain. *Atmospheric Research*, 276, 106246.
- Yuan, L., Zhang, X., Che, Y., Liu, X., Zhao, T. & Song, M. (2022) Vertical profile and radiative forcing of black carbon in a winter pollution period over Chengdu, China. *Atmospheric Research*, 265, 105896.
- Zhang, Q., Shen, Z., Zhang, T., Kong, S., Lei, Y., Wang, Q. et al. (2021) Spatial distribution and sources of winter black carbon and brown carbon in six Chinese megacities. *Science of the Total Environment*, 762, 143075.
- Zhang, Q., Streets, D.G., Carmichael, G.R., He, K.B., Huo, H., Kannari, A. et al. (2009) Asian emissions in 2006 for the NASA INTEX-B mission. *Atmospheric Chemistry and Physics*, 9(14), 5131–5153.
- Zhang, W., Wang, W., Chen, J., Liu, H., Dai, T., Yang, X.Y. et al. (2010) Pollution situation and possible markers of different sources in the Ordos region, Inner Mongolia, China. *Science of the Total Environment*, 408(3), 624–635.
- Zhang, X., Rao, R., Huang, Y., Mao, M., Berg, M.J. & Sun, W. (2015) Black carbon aerosols in urban Central China. *Journal of Quantitative Spectroscopy and Radiative Transfer*, 150, 3–11.
- Zhang, Y., Wu, N., Wang, J., Huang, X., Wang, Z., Liu, T. et al. (2023) Strong haze-black carbon-climate connections observed across northern and eastern China. *Journal of Geophysical Research*, 128(16), e2023JD038505.
- Zhao, D., Liu, D., Yu, C., Tian, P., Hu, D., Zhou, W. et al. (2020) Vertical evolution of black carbon characteristics and heating rate during a haze event in Beijing winter. *Science of the Total Environment*, 709, 136251.
- Zhao, S., Yu, Y., Yin, D., He, J., Liu, N., Qu, J. et al. (2016) Annual and diurnal variations of gaseous and particulate pollutants in 31 provincial capital cities based on in situ air quality monitoring data from China National Environmental Monitoring Center. *Environment International*, 86, 92–106.
- Zheng, H., Kong, S., Chen, N. & Wu, C. (2022) Secondary inorganic aerosol dominated the light absorption enhancement of black carbon aerosol in Wuhan, Central China. *Atmospheric Environment*, 287, 119288.
- Zhu, T., Tang, M., Gao, M., Bi, X., Cao, J., Che, H. et al. (2023) Recent progress in atmospheric chemistry research in China: establishing a theoretical framework for the "air pollution complex". *Advances in Atmospheric Sciences*, 40, 1339–1361.

## SUPPORTING INFORMATION

Additional supporting information can be found online in the Supporting Information section at the end of this article.

**How to cite this article:** Li, Y., Zhang, J., Duan, Q., Kong, X., & Wang, H. (2024). Temporal evolution and source apportionment of BC aerosols during autumn in the grassland of Ordos, China. *Meteorological Applications*, 31(1), e2172. <https://doi.org/10.1002/met.2172>